Research article

Zhiwei Yan, Chong Sheng, Shining Zhu and Hui Liu*

Experimental nanofocusing of surface plasmon polaritons using a gravitational field

https://doi.org/10.1515/nanoph-2020-0059
Received January 27, 2020; accepted April 13, 2020

Abstract: How to capture electromagnetic fields into subwavelength spatial scales has been a major challenge in nanophotonics, especially confining surface plasmon polaritons into regions as small as a few nanometers. Although various methods are proposed to achieve this goal, these methods require complex fabrication process. Here, we demonstrate experimentally the achievement of nanofocusing of surface plasmon polaritons with an intensity enhancement of three, using the simple structure with just pasting a sliver microwire on a sliver layer. And the designed structure has a well-defined gravitational field inspired by transformation optics. This simple design structure has applications to enhance light–matter interactions, such as nonlinear optical process and Raman scattering.

Keywords: gravitational field; nanofocusing; transformation optics.

1 Introduction

Surface plasmon polaritons (SPPs) are the coupled excitations of electromagnetic waves and free-electron, which are surface electromagnetic waves propagating at the metal-dielectric interface. Nanofocusing of SPPs, confining the subwavelength field into regions as small as a few nanometers, has been one of the central goals in the field of nanophotonics, which can enhance light–matter interactions. This prominent capability has numerous applications, e. g., enhanced nonlinear effects [1, 2], nanolasers [3–5], ultraslow light [6], surface-enhanced Raman spectroscopy [7, 8] and plasmonic sensing [9, 10]. To achieve this, various designs, including metallic tips [11], tapered waveguides[12, 13], wedge and V-grooves[14–17], have been demonstrated to realize high spatial field confinement of SPPs.

On the other hand, transformation optics [18–21] based on the coordinate transformation to map the distributions of permittivity and permeability has brought about myriad exotic effects such as invisibility cloaking [22–28], illusion optics [29–32], super-resolution imaging [33, 34], and even mimicking relativity phenomena [35–40]. In addition, transformation optics has also been used to shape plasmonic structures with singularities such as the crescent or kissing cylinders [41–44], where the SPP modes supported slow down as they propagate towards the singularity. One can expect an extremely large field enhancement over a broad frequency spectrum. Alternatively, considerable novel devices have been designed to harvest light by mimicking gravity process based on transformation optics [45–50]. In all these systems, however, it is a big challenge to manufacture complicated metamaterials with strictly-specified position dependent and exceedingly large effective refractive indexes in the lab.

In this work, we have experimentally realized a simple approach for designing a nanofocusing device. By placing a silver microwire on the surface of a silver film, we fabricated a Metal-Insulator-Metal waveguide with a well-defined variable waveguide thickness and hence modulated the effective refractive index of the gap surface plasmon polaritons (GSPP) modes. It is subtle that this GSPP waveguide naturally establishes a precise inverse square law refractive index profile which corresponds to a one-dimensional metric of a gravitational object. Both analytical theory and full-wave numerical simulations demonstrate a good performance of nanofocusing. In our experiment, an obvious nanofocusing effect was observed.

2 Results and discussion

A structured waveguide was fabricated as depicted in Figure 1. During the fabrication process, a polymethyl

***Corresponding author: Hui Liu**, National Laboratory of Solid State Microstructures and School of Physics, Collaborative Innovation Center of Advanced Microstructures, Nanjing University, Nanjing, 210093, Jiangsu, China, E-mail: liuhui@nju.edu.cn. https://orcid.org/0000-0002-0672-1795
Zhiwei Yan, Chong Sheng and Shining Zhu: National Laboratory of Solid State Microstructures and School of Physics, Collaborative Innovation Center of Advanced Microstructures, Nanjing University, Nanjing, 210093, Jiangsu, China

Open Access. © 2020 Zhiwei Yan et al., published by De Gruyter. This work is licensed under the Creative Commons Attribution 4.0 Public License.

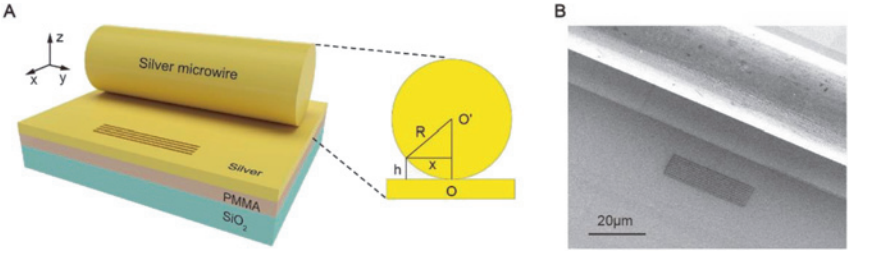

Figure 1: Design of GSPP waveguide for nanofocusing.
(A) Schematic view of the GSPP waveguide formed by placing a silver microwire on a silver film. A grating is used to couple the incident laser into the waveguide. Inset: enlarged schematic of the cross section of the structured GSPP waveguide. (B) SEM image of a fabricated GSPP structure.

methacrylate (PMMA) resist, mixed with oil-soluble Pbs quantum dots, was initially deposited on a silica (SiO_2) substrate. Next, a-80nm-thick silver film was sputtered onto the PMMA surface, followed by a straight silver cylinder (diameter = 25 μm, y-length = 2 mm) glued to it. And then a set of coupling gratings with a period of 750 nm were drilled on the silver film near the silver cylinder with a focused ion beam (FEI Dual Beam HELIOS NANOLAB 600i, 30 keV, 80 pA).We combine the structured waveguide and gap surface plasmon by fixing a silver microwire on the silver film surface. As shown in Figure 1A, when approaching the vicinity of the touching point, the thickness of the air layer can be varied to modulate the effective refractive index of the GSPP modes. Figure 1B presents a scanning electron microscopy (SEM) image of the fabricated GSPPs structure. The grating is 12 um wide (x-length) and 30 um long (y-length). In the x direction, the distance between the center of the grating and the center of the microwire is 30um.

Due to the spatial dependency of the air layer thickness h, its solutions to the Maxwell's equations are difficult to analytically express. However, for simplicity, we can solve it analytically at a fixed positon x where the thickness h is definite. At this point, the structured waveguide can be seen as a simple Metal-Insulator-Metal geometry. Consequently, the dispersion relations to each position of the GSPP waveguide can be obtained. Here, we consider only the symmetric SPP mode of the waveguide [51], which has a dispersion relationship given as

$$\tanh\left(\frac{h\sqrt{\beta^2-k_0^2\varepsilon_d}}{2}\right)+\frac{\varepsilon_d\sqrt{\beta^2-k_0^2\varepsilon_m}}{\varepsilon_m\sqrt{\beta^2-k_0^2\varepsilon_d}}=0 \qquad (1)$$

where β is the propagating wave vector of the SPPs, $\varepsilon_{d(m)}$ are the permittivities of the dielectric(metal) components, and $k_0 = \omega/c$ is the wave vector in free space. Here, we use the Drude model to describe the permittivity of the silver component, given as $\varepsilon_m = \varepsilon_m' + i\varepsilon_m'' = 5 - \omega_p^2/(\omega^2 + i\omega\omega_\tau)$, with plasma frequency $\omega_p = 9.1\,\text{eV}$ and relaxation rate $\omega_\tau = 0.021\,\text{eV}$ [52]. At the same time, ε_d is set to be 1 as the dielectric layer is air. Figure 2A shows the dispersion relations of the GSPPs with air layer thickness h varying from 1 nm to 50 nm. It is obvious that the propagation constant increases as the thickness decreases at a fixed frequency corresponding to 785 nm light indicated by the dashed black line. And the effective refractive index n_{eff} of the GSPP is given by $n_{eff} = \beta/k_0$, which is shown in Figure 2B. Furthermore, both the phase and group velocity of GSPPs asymptotically tend to zero toward the contact point. Consequently, the GSPPs are slowed down and adiabatically stopped at $h \to 0$, leading to their accumulation at the contact point.

Now we try to derive the dependency between the effective index of the GSPP and the lateral distance to the contact point. Due to the cross section of the GSPP structured waveguide, as indicated in the inset of Figure 1A, air layer thickness h decreases as the lateral distance decreases, which can be expressed as

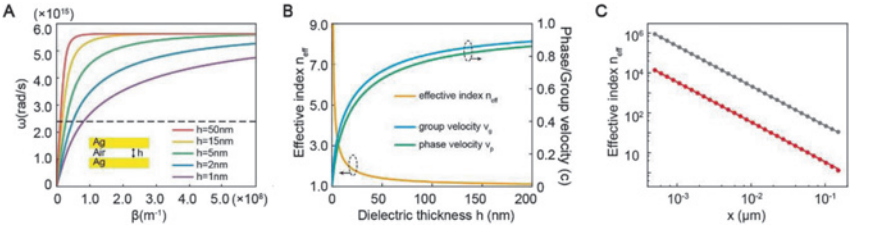

Figure 2: Calculated properties of the GSPP waveguide.
(A) Dispersion relations of the symmetric GSPP modes with air layer thickness h varying from 1 nm to 50 nm. The black dashed line corresponds to the frequency of 785 nm light. (B) Effective refractive index n_{eff}, phase velocity v_p, and group velocity v_g as a function of the air layer thickness h. (C) Effective refractive index n_{eff} as a function of the lateral distance x to the contact point. The black and red lines correspond to the real and imaginary parts of n_{eff} calculated using the approximated result Eq. (2), while the dots are the exact values according to the GSPP dispersion relationship Eq. (1). In (B) and (C) calculations, we have set $\lambda = 785$ nm, $R = 12.5\,\mu$m.

$h(x) = R - \sqrt{R^2 - x^2}$, $(x < R)$, with R the radius of the microwire and x the lateral distance to the contact point. Apparently no analytic form of the effective index can be obtained when substituting $h(x) = R - \sqrt{R^2 - x^2}$ into Eq. (1). However, for sufficiently small air layer thicknesses (when $x/R \ll 1$, $h(x) = R - R(1 - (x/R)^2)^{1/2} \approx x^2/2R \to 0$) and $hk_0 \ll 1$, we can use the approximation $\tanh\left(\frac{h\sqrt{\beta^2 - k_0^2\varepsilon_d}}{2}\right) \approx \frac{x^2\sqrt{\beta^2 - k_0^2\varepsilon_d}}{4R}$ resulting in the following expression

$$n_{eff}(x) \cong n_\infty - \frac{4\varepsilon_d R}{\varepsilon_m k_0 x^2} = n_\infty'\left(1 + \left(\frac{a}{x}\right)^2\right) + in_\infty''\left(1 + \left(\frac{b}{x}\right)^2\right)$$

$$a = \sqrt{-\frac{4R\varepsilon_d\varepsilon_m'}{n_\infty' k_0|\varepsilon_m|^2}},\ b = \sqrt{\frac{4R\varepsilon_d\varepsilon_m''}{n_\infty'' k_0|\varepsilon_m|^2}} \tag{2}$$

where $n_\infty = \sqrt{\varepsilon_d\varepsilon_m/(\varepsilon_d + \varepsilon_m)} = n_\infty' + in_\infty''$ is the asymptotic effective index of the GSPP when h approaches infinity. Note that the effective index near the contact point is inversely square dependent on the lateral distance. We compared the result of the GSPP effective refractive index using Eq. (2) with that rigorously calculated from Eq. (1), which is shown in Figure 2C with solid lines and dots respectively. And both results are in good correspondence.

Here, we intend to identify a curved spacetime whose metric could provide the effective refractive index that we have obtained above. We begin by considering a static centrally symmetric spacetime described by the isotropic metric:

$$ds^2 = d\tau^2 = -g_{00}(r)dt^2 + g_{rr}(r)d\mathbf{x}^2 \tag{3}$$

where g_{00} is the dilation between the proper time τ and the universal time t, $r = |\mathbf{x}|$ is the radial distance, and g_{rr} is a metric that depends on the spatial coordinates $\mathbf{x}$. According to transformation optics that electromagnetic waves propagating in curved space are identical to inhomogeneous medium, we can establish this equation: $n = \sqrt{g_{rr}/g_{00}}$ [45]. Here we take $g_{tt} = 1$, $g_{rr} = n_{eff}^2$. A large variety of gravitational objects in hydrostatic equilibrium can satisfy such a metric, including degenerate star cores such as those in neutron stars, red giants and white dwarfs. When degenerating into one dimension, the metric can provide the exact effective refractive index our GSPP waveguide matches.

And when electromagnetic wave propagating in the curved space, the Helmholtz equation has the form:

$$-\frac{1}{\sqrt{g}}\partial_\beta\sqrt{g}g^{\beta\gamma}\partial_\gamma E^\alpha + \frac{1}{\sqrt{g}}\partial_\beta\sqrt{g}g^{\alpha\gamma}\partial_\gamma E^\beta + \frac{1}{c^2}\frac{\partial^2 E^\alpha}{\partial t^2} = 0 \tag{4}$$

where α, β, γ are space symbol, E^α is electric field and c is velocity of electromagnetic waves . Considering the metric in Eq. (3) and the polarization of SPP $(E^y = \psi(x)e^{ik_0 x})$, the above equation can be written as:

$$\frac{\partial\psi^2(x)}{\partial x^2} - \frac{1}{n_{eff}(x)}\frac{\partial n_{eff}(x)}{\partial x}\frac{\partial\psi(x)}{\partial x} + [n_{eff}(x)k_0]^2\psi(x) = 0 \tag{5}$$

where n_{eff} is given by Eq. (2), $k_0 = \omega/c$.

With the ansatz $n_{eff} \cong n_\infty'\frac{a^2}{x^2}$ when $x \to 0$, the above equation can be written as:

$$\frac{\partial\psi^2(x)}{\partial x^2} + \frac{2}{x}\frac{\partial\psi(x)}{\partial x} + \frac{n_\infty'^2 a^4 k_0^2}{x^4}\psi(x) = 0 \tag{6}$$

Assuming that the envelope ψ is slowly varying $\left(\frac{\partial^2\psi}{\partial x^2} << \frac{\partial\psi}{\partial x}\right)$, we can obtain simplified equation:

$$\frac{\partial\psi(x)}{\partial x} + \frac{n_\infty'^2 a^4 k_0^2}{2x^3}\psi(x) = 0 \tag{7}$$

Then the field intensity of SPP in the gravitation field as:

$$I(x) = |\psi(x)|^2 = I_0 e^{n_\infty'^2 a^4 k_0^2/(4x^2)} = I_0 e^{l_c^2/x^2} \tag{8}$$

Here we define the feature length $l_c = n_\infty' a^2 k_0/2$, and when $x < l_c$ ($l_c \approx 0.89\,\mu$m after considering realistic value), there exist a remarkable enhancement due to the nanofocusing.

To validate the GSPP dynamics in our structured waveguide, full wave simulations are performed using commercial finite-difference time-domain (FDTD) software (Lumerical Solutions, Inc.). Figure 3A shows the simulation results for GSPPs incident towards the contact point. Clearly, the propagation causes accumulation of the GSPPs energy towards the contact point where the local cross-sectional dimension becomes infinitesimally small. The corresponding intensity profile of the GSPPs along the lateral direction is plotted in Figure 3C(blue solid line). The intensity enhances rapidly as GSPPs propagates towards the singularity. The maximum intensity enhancement reaches as high as 10^4. And we fitted the profile with the formula in Eq. (8). In our simulation result, the maximal intensity is not at $x = 0$, which is caused by the mesh size limitation at this point during the simulation. But the trend of the enhanced intensity caused by nanofocusing fits the formula Eq. (8) well.

In the experiment, we focused a 785 nm laser light on the grating coupler parallel to the microwire by a microscope objective (Olympus Plan Achromat Objective

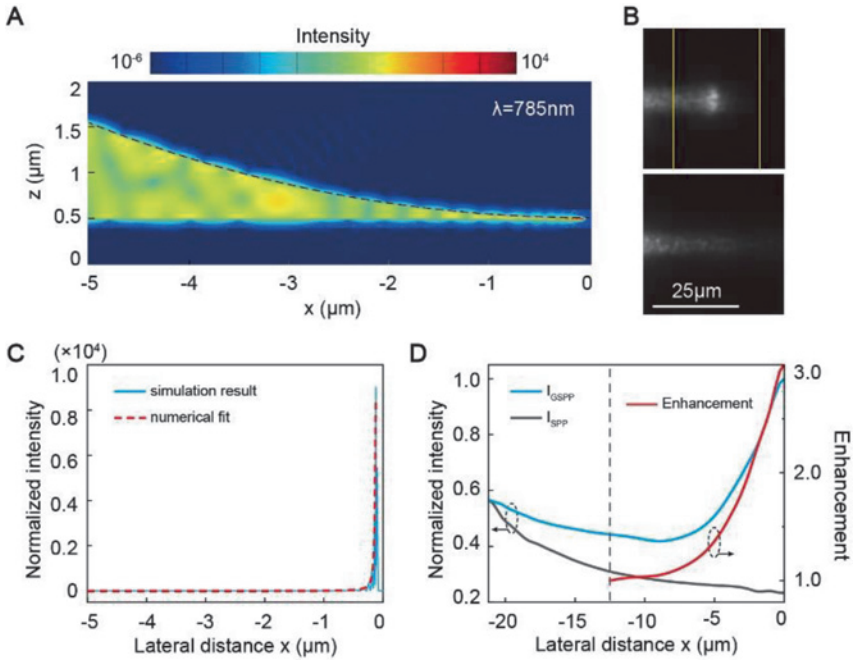

Figure 3: Simulation and experimental results.
(A) Full wave simulation of GSPP propagation. In the simulation we have fixed $\lambda = 785$ nm, $R = 12.5\,\mu$m. The location of the microwire is indicated with dashed black line. (B) Top-view camera images of the propagation behavior of the SPPs with (top) and without (bottom) the presence of a silver microwire. The yellow lines indicate the position of the microwire. (C) Normalized intensity profile as a function of the lateral distance x. The blue solid line is simulation result obtained from (A), and the red dashed line shows the numerical fitting result in the form of Eq. (8). (D) Normalized intensity profiles of the SPPs extracted from (B). The blue line shows the dramatic enhancement intensity of GSPPs when propagating, while the grey one indicates the attenuation of an ordinary SPP. The red line is the enhancement defined as $\frac{I_{GSPP}/I_{GSPP}(x_0)}{I_{SPP}/I_{SPP}(x_0)}$, where x_0 is at the radius of the microwire in the x direction which is indicated by the vertical black dashed line.

20×/0.4) and stimulated the SPP mode in the GSPP waveguide. The spot size of the incident light is about 10um. As the SPPs propagate towards the contact point, it excites the quantum dots inside the PMMA layer, which re-emit fluorescent light at 1050 nm to demonstrate the propagation behavior of the SPPs. The fluorescence was collected by a microscope objective (Zeiss Epiplan × 50/0.17 HD microscope objective) and delivered to a charge-coupled device camera. Figure 3B shows the obtained fluorescence image. Clearly, when the GSPPs propagate towards the contact point, the field enhancement is significant, which indicates that the energy of the GSPP mode was extremely concentrated between the microwire and the silver film inside the air layer. Furthermore, the image also shows that the GSPPs nearly stopped at the contact point due to the sharp decrease of the phase and group velocity. For comparison, the image of an ordinary SPP is depicted whose intensity attenuated gradually during the propagation. We extracted the normalized intensity of both cases displayed in Figure 3D. When propagating the same distance, the intensity of the GSPPs at the contact point was more than three times stronger than the intensity of an ordinary SPP. By comparing the experimental enhancement in Figure 3D and the simulation enhancement in Figure 3C, the experimental result is much smaller. And the limited enhancement is caused by some experimental technique and physical mechanism. On the one hand, the surface roughness of silver and microwire in our experiment is about 10 nm and even larger, we cannot obtain the ideal case that gap size is nearly zero just as in the simulation. Besides that, we take quantum dot to absorb the energy of SPPs for fluorescence imaging, which also vitiates the enhancement process during the nanofocusing. On the other hand, the quantum nature of sliver, such as electron spill-out and nonlocal effect, and intrinsic loss of sliver play a role to restrict the large enhancement in real experiment.

Since this design of GSPP waveguide intensifies light by nanofocusing it into sub-wavelength spatial scales, we expect that it can be used to enhance nonlinear optical process such as second-harmonic (SH) generation. Based on the structure in Figure 1A, we embedded an extra dielectric layer (thickness = 10 nm) of lithium niobate ($LiNbO_3$, LN), which possesses large $\chi^{(2)}$ nonlinear coefficients [53], between the silver film and the silver microwire, as shown in the inset of Figure 4A. Full wave nonlinear simulations using commercial finite-difference time-domain (FDTD) software (Lumerical Solutions, Inc.) were conducted to demonstrate how this GSPP waveguide yields field enhancement for SH generation. In the simulation, a 785 nm source was incident toward the touching point. Figure 4A shows the generated SH signal, revealing a strong nonlinear response in close proximity to the contact point. We plotted the electric field intensity of both the fundamental light and the SH light in Figure 4B. Clearly, they both undergo a substantial boost in the close vicinity of the singular point. The same process occurs at another

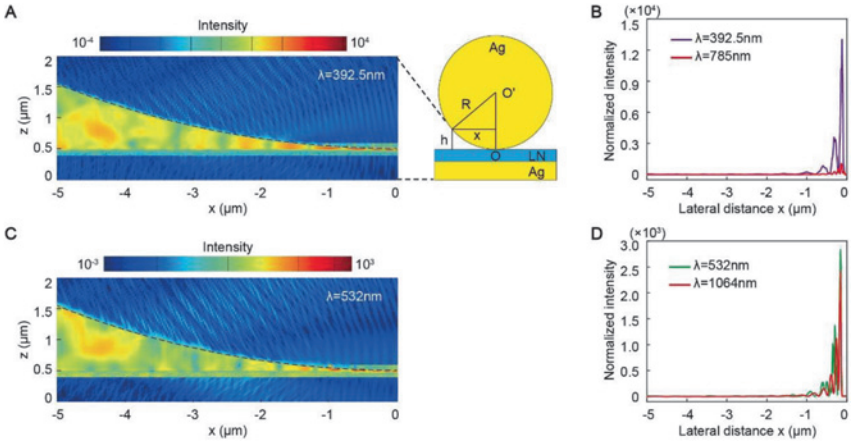

Figure 4: FDTD Simulation of enhanced SH generation.
(A) Electric field intensity distributions of the SH signal (λ = 392.5 nm). In the simulation we have fixed the incident fundamental light λ = 785 nm and the microwire R = 12.5 μm. The location of the microwire is indicated with dashed black line. The right panel is the schematic of the cross section of the new setup GSPP waveguide, where the LN layer thickness is 10 nm. (B) Normalized intensity profile of the fundamental 785 nm light (red line) and the SH 392.5 nm light (purple line) as a function of the lateral distance x. (C) Electric field intensity distributions of the SH signal (λ = 532 nm) when the incident fundamental light is set as λ = 1064 nm. (D) Normalized intensity profile of the fundamental 1064 nm light (red line) and the SH 532 nm light (green line) as a function of the lateral distance x.

arbitrarily chosen fundamental wavelength λ = 1064 nm, which is shown in Figures 4C and D, indicating a broadband enhanced second-order nonlinear optical process. Since the nonlinear interaction strength is proportional to the light intensity, our design has the potential to realize broadband and enhanced SH generation. In our experiment, due to the restriction of loss, the enhancement of fundamental light is much smaller than the simulation one. This limited enhancement may not produce the threshold required for nonlinear processes.

3 Conclusion

In conclusion, we have experimentally demonstrated adiabatic nanofocusing of electromagnetic radiation within deep subwavelength regime without complex nanofabrication technology using a sliver microwire placing on sliver layer. Furthermore, the nanofocusing process can be clearly manifested by fluorescence measurement with an intensity enhancement as large as three. We believe that this simple designed structure will be valuable for capturing electromagnetic waves into subwavelength regime to enhance light–matter interactions, such as nonlinear optical process and Raman scattering.

Acknowledgments: This work was financially supported by the National Natural Science Foundation of China (Nos. 11690033, 61425018, 11621091, and 11704181), National Key R&D Program of China (Nos. 2017YFA0303702, 2017YFA0205700).
Author contribution: All the authors have accepted responsibility for the entire content of this submitted manuscript and approved submission. Zhiwei Yan and Chong Sheng contributed equally to this paper.
Research funding: The research was funded by National Natural Science Foundation of China (Nos. 11690033, 61425018, 11621091, and 11704181), National Key R&D Program sof China (Nos. 2017YFA0303702 and 2017YFA0205700).
Employment or leadership: None declared.
Honorarium: None declared.
Conflict of interest statement: The authors declare no conflicts of interest regarding this article.

References

[1] I. Y. Park, S. Kim, J. Choi, et al., "Plasmonic generation of ultrashort extreme-ultraviolet light pulses," *Nat. Photon.*, vol. 5, pp. 677–681, 2011.
[2] M. P. Nielsen, X. Shi, P. Dichtl, S. A. Maier, and R. F. Oulton, "Giant nonlinear response at a plasmonic nanofocus drives efficient four-wave mixing," *Science*, vol. 358, pp. 1179–1181, 2017.
[3] D. J. Bergman and M. I. Stockman, "Surface plasmon amplification by stimulated emission of radiation: Quantum generation of coherent surface plasmons in nanosystems," *Phys. Rev. Lett.*, vol. 90, Art no. 027402, 2003.
[4] T. Pickering, J. M. Hamm, A. F. Page, S. Wuestner, and O. Hess, "Cavity-free plasmonic nanolasing enabled by dispersionless stopped light," *Nat. Commun.*, vol. 5, p. 4972, 2014.
[5] M. T. Hill and M. C. Gather, "Advances in small lasers," *Nat. Photon.*, vol. 8, pp. 908–918, 2014.
[6] K. L. Tsakmakidis, O. Hess, R. W. Boyd, and X. Zhang, "Ultraslow waves on the nanoscale," *Science*, vol. 358, Art no. eaan5196, 2017.
[7] T. Ichimura, , N. Hayazawa, , M. Hashimoto, , Y. Inouye, , Kawata, S., 2004. Tip-enhanced coherent anti-stokes raman scattering for vibrational nanoimaging. Phys. Rev. Lett. 92, 220801.
[8] D. A. Genov, A. K. Sarychev, V. M. Shalaev, and A. Wei, "Resonant field enhancements from metal nanoparticle arrays," *Nano Lett.*, vol. 4, pp. 153–158, 2004.
[9] Genov, D.A., Oulton, R.F., G. Bartal, , X. Zhang, , 2011. Anomalous spectral scaling of light emission rates in low-dimensional metallic nanostructures. Phys. Rev. B 83, 245312.

[10] J. O. Arroyo and P. Kukura, "Non-fluorescent schemes for single-molecule detection, imaging and spectroscopy," *Nat. Photon.*, vol. 10, pp. 11–17, 2016.
[11] C. Ropers, C. C. Neacsu, T. Elsaesser, M. Albrecht, M. B. Raschke, and C. Lienau, "Grating-coupling of surface plasmons onto metallic tips: A nanoconfined light source," *Nano Lett.*, vol. 7, pp. 2784–2788, 2007.
[12] M. I. Stockman, "Nanofocusing of optical energy in tapered plasmonic waveguides," *Phys. Rev. Lett.*, vol. 93, Art no. 137404, 2004.
[13] H. Choo, M. K. Kim, M. Staffaroni, et al., "Nanofocusing in a metal–insulator–metal gap plasmon waveguide with a three-dimensional linear taper," *Nat. Photon.*, vol. 6, pp. 838–844, 2012.
[14] K. C. Vernon, D. K. Gramotnev, and D. F. P. Pile, "Adiabatic nanofocusing of plasmons by a sharp metal wedge on a dielectric substrate," *J. Appl. Phys.*, vol. 101, Art no. 104312, 2007, https://doi.org/10.1063/1.2732699.
[15] Davoyan, A.R., Shadrivov, I.V., Zharov, A.A., Gramotnev, D.K., Kivshar, Y.S., 2010. Nonlinear nanofocusing in tapered plasmonic waveguides. Phys. Rev. Lett. 105, 116804. https://doi.org/10.1103/physrevlett.105.116804.
[16] S. I. Bozhevolnyi, and K. V. Nerkararyan, "Adiabatic nanofocusing of channel plasmon polaritons," *Opt. Lett.*, vol. 35, pp. 541–543, 2010.
[17] X. P. Shen and T. J. Cui, "Ultrathin plasmonic metamaterial for spoof localized surface plasmons," *Laser Photon. Rev.*, vol. 8, pp. 137–145, 2014.
[18] J. B. Pendry, D. Schurig, and D. R. Smith, "Controlling electromagnetic fields," *Science*, vol. 312, pp. 1780–1782, 2006.
[19] U. Leonhardt, "Optical conformal mapping, "*Science*, vol. 312, pp. 1777–1780, 2006.
[20] H. Y. Chen, C. T. Chan, and P. Sheng, "Transformation optics and metamaterials," *Nat. Mater.*, vol. 9, pp. 387–396, 2010.
[21] L. Xu and H. Y. Chen, "Conformal transformation optics, "*Nat. Photon.*, vol. 9, pp. 15–23, 2015.
[22] D. Schurig, J. J. Mock, B. J. Justice et al., "Metamaterial electromagnetic cloak at microwave frequencies," *Science*, vol. 314, pp. 977–980, 2006.
[23] W. S. Cai, U. K. Chettiar, A. V. Kildishev, and V. M. Shalaev, "Optical cloaking with metamaterials," *Nat. Photon.*, vol. 1, pp. 224–227, 2007.
[24] H. Chen, B. I. Wu, B. Zhang, and J. A. Kong, "Electromagnetic wave interactions with a metamaterial cloak," *Phys. Rev. Lett.*, vol. 99, Art no. 063903, 2007.
[25] Li, J.S., Pendry, J.B., 2008. Hiding under the carpet: A new strategy for cloaking. Phys. Rev. Lett. 101, 203901.
[26] U. Leonhardt, and T. Tyc, "Broadband invisibility by non-euclidean cloaking," *Science*, vol. 323, pp. 110–112, 2009.
[27] Y. Lai, H. Chen, Z. Q. Zhang, and C. T. Chan, "Complementary media invisibility cloak that cloaks objects at a distance outside the cloaking shell," *Phys. Rev. Lett.*, vol. 102, Art no. 093901, 2009.
[28] Y. Ma, , Y. Liu, , M. Raza, , Y. Wang, , S. He, , 2014. Experimental demonstration of a multiphysics cloak: Manipulating heat flux and electric current simultaneously. Phys. Rev. Lett. 113, 205501.
[29] Lai, Y., J. Ng, , Chen, H.Y., et al., 2009. Illusion optics: The optical transformation of an object into another object. Phys. Rev. Lett. 102, 253902.
[30] F. Zolla, S. Guenneau, A. Nicolet, and J. B. Pendry, "Electromagnetic analysis of cylindrical invisibility cloaks and the mirage effect," *Opt. Lett.*, vol. 32, pp. 1069–1071, 2007.
[31] Li, C., Meng, X.K., Liu, X.A., et al., 2010. Experimental realization of a circuit-based broadband illusion-optics analogue. Phys. Rev. Lett. 105, 233906.
[32] W. X. Jiang, C. W. Qiu, T. C. Han, S. Zhang, and T. J. Cui, "Creation of ghost illusions using wave dynamics in metamaterials," *Adv. Funct. Mater.*, vol. 23, pp. 4028–4034, 2013.
[33] I. I. Smolyaninov, Y. J. Hung, and C. C. Davis, "Magnifying superlens in the visible frequency range," *Science*, vol. 315, pp. 1699–1701, 2007.
[34] Z. W. Liu, H. Lee, Y. Xiong, C. Sun, and X. Zhang, "Far-field optical hyperlens magnifying sub-diffraction-limited objects," *Science*, vol. 315, pp. 1686–1716, 2007.
[35] A. Greenleaf, , Y. Kurylev, , M. Lassas, , G. Uhlmann, , 2007. Electromagnetic wormholes and virtual magnetic monopoles from metamaterials. Phys. Rev. Lett. 99, 183901.
[36] Smolyaninov, I.I., Narimanov, E.E., 2010. Metric signature transitions in optical metamaterials. Phys. Rev. Lett. 105, 67402.
[37] T. G. Mackay and A. Lakhtakia, "Towards a metamaterial simulation of a spinning cosmic string," *Phys. Lett.*, vol. 374, pp. 2305–2308, 2010.
[38] V. Ginis, P. Tassin, B. Craps, and I. Veretennicoff, "Frequency converter implementing an optical analogue of the cosmological redshift," *Optics Express*, vol. 18, pp. 5350–5355, 2010.
[39] I. I. Smolyaninov and Y. J. Hung, "Modeling of time with metamaterials," *J. Opt. Soc. Am. B*, vol. 28, pp. 1591–1595, 2011.
[40] Q. Cheng, T. J. Cui, W. X. Jiang, and B. G. Cai, "An omnidirectional electromagnetic absorber made of metamaterials," *New J. Phys.*, vol. 12, Art no. 063006, 2010.
[41] J. B. Pendry, A. Aubry, D. R. Smith, and S. A. Maier, "Transformation optics and subwavelength control of light," *Science*, vol. 337, pp. 549–552, 2012.
[42] J. B. Pendry, A. I. Fernandez-Dominguez, Y. Luo, and R. K. Zhao, "Capturing photons with transformation optics," *Nat. Phys.*, vol. 9, pp. 518–522, 2013.
[43] J. B. Pendry, Y. Luo, and R. K. Zhao, "Transforming the optical landscape," *Science*, vol. 348, pp. 521–524, 2015.
[44] A. Aubry, D. Y. Lei, A. I. Fernandez-Dominguez, Y. Sonnefraud, S. A. Maier, and J. B. Pendry," Plasmonic light-harvesting devices over the whole visible spectrum," *Nano Lett.*, vol. 10, pp. 2574–2579, 2010.
[45] D. A. Genov, S. Zhang, and X. Zhang, "Mimicking celestial mechanics in metamaterials," *Nat. Phys.*, vol. 5, pp. 687–692, 2009.
[46] E. E. Narimanov and A. V. Kildishev, "Optical black hole: Broadband omnidirectional light absorber," *Appl. Phys. Lett.*, vol. 95, Art no. 041106, 2009.
[47] Q. Cheng, T. J. Cui, W. X. Jiang, and B. G. Cai, "An omnidirectional electromagnetic absorber made of metamaterials," *New J. Phys.*, vol. 12, Art no. 063006, 2010.
[48] K. V. Nerkararyan, S. K. Nerkararyan, and S. I. Bozhevolnyi, "Plasmonic black-hole: Broadband omnidirectional absorber of gap surface plasmons," *Opt. Lett.*, vol. 36, pp. 4311–4313, 2011.
[49] C. Sheng, H. Liu, Y. Wang, S. N. Zhu, and D. A. Genov, "Trapping light by mimicking gravitational lensing," *Nat. Photon.*, vol. 7, pp. 902–906, 2013.

[50] L. Shen, L. J. Prokopeva, H. Chen, and A. V. Kildishev, "Designing optimal nanofocusing with a gradient hyperlens," *Nanophotonics*, vol. 7, pp. 479–487, 2018.
[51] S. A. Maier, *Plasmonics: Fundamentals and Applications*, Berlin, Germany. Springer Science & Business Media, 2007.
[52] E. D. Palik, *Handbook of Optical Constants of Solids*, Cambridge, Massachusetts, US. Academic Press, 1998.
[53] I. Shoji, T. Kondo, A. Kitamoto, M. Shirane, and R. Ito, "Absolute scale of second-order nonlinear-optical coefficients," *J. Opt. Soc. Am. B*, vol. 14, pp. 2268–2294, 1997.